Motor injury is caused by TBK1 deficiency in the myeloid cell and rescued by PEI-manose-TBK1

Weisong Duan
neurology
Le Yi
neurology
Yunyun Tian
neurology
Huai-peng Huang
pingan hospital
Zhongyao Li
neurology
Yue Bi
neurology
Moran Guo
neurology
Yuanyuan Li
neurology
Yakun Liu
neurology
Yanqin Ma
jiangsu Ehwa
Xueqin Song
neurology
Yaling Liu
neurology
Chunyan Li (hebeichunyanli@aliyun.com)
Department of Neurology,The Second Hospital of Hebei Medical University

---

Research

Keywords: Tbk1, Frontotemporal dementia, Amyotrophic lateral sclerosis, Macrophage

Posted Date: March 25th, 2020

DOI: https://doi.org/10.21203/rs.3.rs-17978/v1

Abstract

Background: TBK1 haploinsufficiency has been shown to cause both amyotrophic lateral sclerosis (ALS) and frontotemporal dementia (FTD); however, the mechanism is unclear.

Methods: A myeloid Tbk1 knockout mice (Tbk1-LKO mice) was established. Motor functional and pathological analyses were also performed. The p-TBK1 was tested by flow cytometry in the ALS animal model and patients. The inflammatory proteins and mRNA was analyzed by Western blot and RT-PCR.

Results: We found that the latency to fall in seven-month-old Tbk1-LKO mice was significantly reduced on evaluation on two consecutive days. Overall, 25.6% of Tbk1-LKO mice presented paralysis symptoms and signs along with a loosened myelin sheath and axon degeneration at 14-16 months of age. Furthermore, Tbk1 deficiency in myeloid cells induced inflammatory cell infiltration and dysbacteriosis in the digestive tract. Additionally, p-Tbk1 content was reduced by 29.5% and 14.8% in monocytes of definite ALS and probable ALS patients and decreased by 27.6% and 45.5% in the monocytes and microglia of ALS animals, respectively. PEI-mannose-TBK1 or PEI-mannose-SaCas9-sgRNA for deleting mutant SOD1 in macrophages significantly delayed disease onset and prolonged survival in the ALS mouse model.

Conclusions: These data suggest that inflammatory monocyte and macrophage infiltration and impaired innate immune defense are contributing factors to ALS and FTD.

Background

Amyotrophic lateral sclerosis (ALS) is a fatal neurodegenerative disease characterized by progressive loss of motor neurons in the cortex, brain stem, and spinal cord[1–2]. TANK-binding kinase1 (Tbk1) haploinsufficiency mutations have been shown to contribute to the pathogenesis of ALS and frontotemporal dementia (FTD)[3–7].

TBK1, a member of the IκB kinase (IKK) family, regulates immune defense during microorganism intrusion[8]. TBK1 phosphorylates IRF3 and upregulates IFN-beta for defense against virus infection in the innate immune signaling pathway[9]. TBK1 controls energy metabolism by inducing the degradation of the IKK kinase NIK in adipocytes[10], and is also involved in the insulin resistance mechanism related to IR Ser994 phosphorylation in a genetic model of diabetes [11]. Tbk1 germline knockout (KO) mice die embryonically at E14.5 due to liver degeneration[12]. The recent generation of Tbk1 conditional KO mice has demonstrated that Tbk1 maintains the immune balance in the body[13–15]. Our previous study demonstrated that Tbk1 deletion in neuron progenitor cells caused mild cognitive and locomotor deficits[16]. Additionally, several studies have supported the hypothesis that a human endogenous retrovirus in motor neurons is activated in ALS patients[17–18]. Therefore, we speculated that deleting Tbk1 in phagocytes, as the first defense against microorganism attack, could be facilitate ALS pathogenesis.

Methods

Study cohort

All patients were diagnosed according to the El-Escorial criteria for definite and probable ALS. Patients were considered sporadic based upon a negative family history. Individuals with confounding conditions affecting the immune system were excluded. Age- and sex-matched healthy controls were chosen, as listed in Table s1.

Animal models

$Tbk1^{fl/fl}$ mice were generated by Taconic, and $SOD1^{G93A}$ transgenic mice (B6SJL-TgN [SOD1-G93A] 1Gur) were obtained from Jackson Laboratories. $Tbk1^{fl/fl}$ mice were crossed with LysM-cre mice to generate $Tbk1^{fl/fl}$ LysM-cre (termed Tbk1-LKO) and $Tbk1^{fl/fl}$ WT mice. Animals were bred and maintained under controlled conditions (12-h light/dark cycles, 60% ± 10% relative humidity, 22 ± 1°C). The copy number of the hSOD1 gene was evaluated by real-time PCR. Body weight was measured every 7 days, starting at approximately 60 days of age.

Animal experiments were carried out according to the laboratory animal management regulations promulgated by the Ministry of Science and Technology of the People's Republic of China, which are in accordance with the NIH Guide for the Care and Use of Laboratory Animals.

PEI-mannose packaging

According to the protocol of In vivo-jetPEI®-Man (Polyplus transfection), the nucleic acids, including TBK1 plasmid and AAV-SaCas9-sgRNA targeting SOD1, and reagent were separately diluted in a 5% glucose solution and then mixed together, and after a 15 min incubation at room temperature (RT), the nucleic acid/in vivo-jetPEI®-Man complexes were injected into the animals via the tail vein.

Cell culture

The NSC-34 cell line was routinely maintained in DMEM (Invitrogen, CA, USA; cat. No: 21063-029) supplemented with 10% heat-inactivated FBS (Invitrogen; cat. No: 16000-044) and antibiotics (100 IU/mL penicillin and 100 μg/mL streptomycin).

THP-1 cells were routinely maintained in RPMI-1640 medium (Gibco, 8119144) supplemented with 10% heat-inactivated FBS (Invitrogen; cat. No: 16000-044) and antibiotics (100 IU/mL penicillin and 100 μg/mL streptomycin).

Human primary monocyte culture

After written informed consent was obtained, we collected peripheral blood from subjects. Human primary PBMCs were isolated with HISTOPAQUE-1077 (Sigma-Aldrich) according to the manufacturer's protocols. Cells were maintained in RPMI-1640 medium (Gibco, 8119144) supplemented with 10%

(vol/vol) FBS, 2 mM glutamine, penicillin (100 U/mL) and streptomycin (100 mg/mL). For monocyte differentiation into macrophages, M-CSF (20 ng/mL, Sino Biological, 11792-H08H) was added for 7 days.

Inhibitors and activators

Amlexanox (LKT Labs, A4944), Nik smi1 (MCE, HY-112433), BV6 (MCE, HY-16701), human TNF alpha (Sino Biological, 10602-HNAE), and mouse Tnf alpha (Sino Biological, 50349-MNAE) were used.

Immunohistochemistry

Following transcardiac perfusion with 4% paraformaldehyde, mouse tissues were removed and further fixed for 24 h in the same fixative, followed by paraffin embedding. The tissue was cut into 5 μm sections. The sections were permeabilized with 0.3% Triton X-100 and then washed three times in 0.01 M phosphate-buffered saline (PBS). After blocking with 3% H_2O_2 in methanol for 15 min and in 10% horse serum for 1 h at RT, the sections were incubated overnight at 4℃ with antibodies against IBA1 (1:500, Wako, 019-19741), Chat (1:500, Abcam, 178850), NeuN (1:500, Millipore, MAB377), CD11B (1:100, Proteintech, 20991-1-AP), Arginase1 (1:100, Proteintech, 16001-1-AP), or GFAP (1:200, Millipore, MAB360). The sections were subsequently incubated at RT with a biotin-conjugated secondary antibody (ZSGB-BIO, 1:200) for 2 h, followed by incubation with HRP-conjugated streptavidin (ZSGB-BIO, 1:200) for 1 h and 0.03% diaminobenzidine as a chromogen for 10 min. Slides were mounted and analyzed by light microscopy (Olympus BX51).

Muscle morphology

Ten-micron frozen cross-sections were stained with HE, and the stained sections were visualized using an Olympus microscope (BX53). Images were captured with a digital camera and analyzed using image analysis software (DP73). Approximately 300 fibers of the gastrocnemius were recorded, and the fiber area was calculated using ImageJ.

Confocal laser scanning microscopy

Spinal cord sections (obtained as described above) were washed three times in 0.3% Triton X-100/PBS and blocked in 10% horse serum for 30 min. Primary antibodies against P100 (1:100, Cell Signaling, 4882), Neu N (1:100, Millipore, MAB377), GFAP (1:200, Millipore, MAB360), phospho-Tbk1 (1:50, Cell Signaling, 5483), and IBA1 (1:200, Wako, 019-19741) were applied overnight at 4℃. After washing, the sections were incubated with fluorescent secondary antibodies for 1 h at RT. The slides were observed using confocal fluorescence microscopy (Olympus FV1000).

Western blotting

Protein expression in the cortex and cerebellum was quantified by western blotting. Total protein was extracted using a total protein extraction kit (Applygen Technologies Inc., P1250). Fifty micrograms of protein from each sample was separated on a 10% or 12% SDS-PAGE gel and transferred onto PVDF

membranes. The membranes were incubated overnight at 4°C with primary antibodies, including those against β-actin (1:2000, Proteintech, 60008-1-Ig), CD11B (1:1000, Proteintech, 20991-1-AP), P100 (1:1000, Cell Signaling, 4882), Arginase1 (1:1000, Proteintech, 16001-1-AP), GAPDH (1:5000, Proteintech, 10494), or hSOD1 (1:10000, Abcam, ab51254). Following incubation with fluorescent secondary antibodies for 1 h at RT, an Odyssey Infrared Imaging System (LI-COR, Lincoln, NE) was used to detect the bands of interest.

Quantitative RT-PCR

Copy number: DNA was isolated from the mouse tail using an extraction kit (Generay Biotechnology, Shanghai, China) according to the manufacturer's instructions. Quantitative PCR was performed using synthetic primers, SYBR Green (Generay Biotech Co., Ltd., GK8020) and an M3005P system (Agilent Technologies, Santa Clara, CA, USA). The following sequences were used in this assay: hSOD1, 5'-CATCAGCCCTAATCCATCTGA-3' (forward) and 5'-CGCGACTAACAATCAAAGTGA-3' (reverse); and mIL2, 5'-CTAGGCCACAGAATTGAAAGATCT-3' (forward) and 5'-GTAGGTGGAAATTCTAGCATCATCC-3' (reverse). The amplification conditions were as follows: 95°C for 10 min followed by 40 cycles of amplification at 95°C for 30 s, 60°C for 1 min, and 72°C for 30 s. The difference in CT (ΔCT) values was computed as the difference between the human SOD1 CT value and the mouse IL2 CT value (ΔCT=mIL2 CT-hSOD1 CT).

Total RNA was isolated from the tissues using an RNA rapid extraction kit (Generay Biotech Co., Ltd., GK3016) in accordance with the manufacturer's protocol. cDNA was prepared using AMV reverse transcriptase and random primers (Promega, A3500). Targeted gene primers and SYBR Green (Generay Biotech Co., Ltd., GK8020) were used for quantitative PCR on an M3005P (Agilent Technologies, Santa Clara, USA). After incubating the samples at 95°C for 10 min, 40 cycles of amplification at 95°C for 10 s, 60°C for 20 s, and 72°C for 15 s were performed. GAPDH was used as a reference gene. The synthesized primers used here are listed in Table s2.

Flow cytometry

Osmotic lysis of red blood cells was performed using 45 mL of RBLB (red blood cell lysis buffer: 50 mM NH4Cl, 70 mM NaHCO3, 0.1% EDTA, ddH2O) for 5 mL of whole blood for 10 min at RT. Leukocytes were centrifuged for 5 min at 500×g at 4°C and washed twice in PBS. Leukocytes were resuspended in 400 μL of PBS and stained with antibodies specific for cell surface antigens (CD11B-FITC, 1:100, BD, 557396; Ly6c-APC, 1:100, eBioscience, 17-5932-82; CD206-PE, 1:100, eBioscience, 12-2061-82; F4/80-APC, 1:100, eBioscience, 17-4801; CD14-APC, 1:100, BD, 555399; and CD16-perCY-CY5.5, 1:100, BD, 560717) for 30 min on ice in the dark. After washing in PBS, the stained cells were fixed and permeabilized by adding 500 μL of Fixation/Permeabilization solution (Cytofix/Cytoperm^{TM} Plus Fixation/Permeabilization Kit, BD, 554714) and incubated at RT in the dark for 20 min. Thoroughly resuspended fixed/permeabilized cells were incubated with p-TBK1-PE (1:100, Cell Signaling, 13498) at 4°C for 30 min in the dark. After washing cells twice with 1×BD Perm/Wash^{TM} buffer and resuspending in staining buffer, flow cytometric analysis was then performed.

Electron microscopy

Tissues were fixed in 4% glutaraldehyde and treated with 1% OsO_4 in 0.1 M PBS. The samples were dehydrated through graded acetone solutions and embedded in EPON 812. Ultrathin sections (70 nm) were placed on a copper grid and stained with uranyl acetate and lead citrate. The samples were observed by transmission electron microscopy (TEM, JEM-1230).

Bielschowsky staining

Staining of nerve fibers was carried out using a Hito Bielschowsky OptimStain Kit (HTKNS1126). Briefly, the slides were incubated with Solution 1 for 15 min, followed by immersion in the Developer solution for 1-8 min until the tissues became golden-brown. After incubation with Solution 4, sections were rinsed with distilled water, dehydrated, cleared, and coverslipped.

Motor function test

A rotarod (Rota-Rod; Ugo Basile, Gemonio, Italy) was used to assess motor function in mice. With an arbitrary cut-off time of 180 s, three once-per-week trials were performed, and the longest time was recorded. The onset of disease was determined as a reduction in rotarod performance between weekly time points. The weight of the mice was measured every 7 days, starting at 60 days of age.

Accelerated rotarod testing. Mice were placed on the top of the revolving beam for 4 successive trials/day for 2 days, with 20-min intertrial intervals. The rod was accelerated gradually from 4 to 28 rpm over 2 min. Latencies before falling from the rod were recorded.

The footprints of the mice were recorded during continuous locomotion. The stride length was measured as the distance between footprints, and the average stride length was calculated from three stride lengths.

The weight of the mice was measured every 7 days, starting at 60 days of age.

Microbiota analysis

Total DNA was extracted from the feces of mice. PCRs targeting the V3-V4 regions of the 16S rDNA genes (probes used: 319F, 5’-ACTCCTACGGGAGGCAGCAG-3’ and 806R, 5’-GGACTACHVGGGTWTCTAAT-3) were performed, and sequencing reactions were performed using Illumina HiSeq sequencing technology for paired-end reads. Paired-end reads obtained were merged using FLASH v1.2.11 software, and reads with a length ≥ 400 bp were kept for the following analysis. The merged sequences were processed with QIIME v1.8.0, and the sequences were binned into operational taxonomic units (OTUs) based on 97% identity. Alpha diversity, richness, Venn diagrams, heat maps, principal coordinate analysis, and linear discriminant analysis were further processed with a bioinformatic pipeline tool, BMK Cloud online (Biomarker Technologies Corporation, Beijing, China).

Statistical analysis

Data were analyzed using SPSS 13.0 software. Lifespan was compared between groups of mice by the Kaplan–Meier method. Comparisons among multiple groups were performed using one-way ANOVA followed by Student–Newman–Keuls or Dunn's T tests. All values are expressed as the mean ± S. E., and $P < 0.05$ was considered statistically significant.

Results

Tbk1-LKO leads to motor injury

Recent works strongly support that TBK1 haploinsufficiency causes neurodegeneration, including ALS and FTD. It is well known that TBK1 plays a pivotal role in the innate immune response against virus infection. Therefore, we generated Tbk1 conditional KO mice by crossing Tbk1-flox mice[10] with LysMcre mice expressing Cre in the myeloid cells that induce the innate immune response. The resulting $Tbk1^{fl/fl}$ LysMcre (hereafter called Tbk1-LKO) mice and $Tbk1^{fl/fl}$ wild-type (WT) control mice were genotyped by PCR (Figure 1A). Flow cytometry analyses readily detected that the rate of p-Tbk1 in the ly6c-positive monocytes of WT mice was 5.6%; however, that in the Tbk1-LKO mice was 0.4% (Figure 1B). To assess the behavioral impact of Tbk1 deletion, locomotor function was evaluated by the rotarod test in Tbk1-LKO and age-matched WT mice. Seven-month-old Tbk1-LKO mice exhibited a significantly reduced latency to fall on evaluation on two consecutive days (WT on day one: 179.4±17.84 s, Tbk1-LKO on day one: 122.2 ±20.04 s; WT on day two: 222.6±11.86 s, Tbk1-LKO on day two: 165.6 ±24.92 s; Figure 1C). To determine whether the locomotor damage in the Tbk1-LKO mice deteriorated with increasing age, the common conditions of thirty-nine Tbk1-LKO mice were recorded until the cut-off age of 14-16 months (Figure s1A). Overall, 25.6% of Tbk1-LKO mice presented paralysis, abnormal footprints and stretch width, weight loss and shortened survival (Figure 1D-I, Figure s1A). Furthermore, as shown in Figure 1J and Figure s1B, the gastrocnemius fiber area was reduced by 24% in the Tbk1-LKO mice compared with that in WT mice. We hypothesized that Tbk1 deletion could result in motor neuron degeneration and gliosis in the spinal cord. Surprisingly, we did not find degenerated motor neurons or activated microglia or astrocytes in the spinal cord (Figure s2A-C). Subsequently, sciatic nerve staining was performed, including toluidine blue staining, Bielschowsky staining and osmic acid staining, which demonstrated that the myelin sheath was dramatically loosened, with axon degeneration (G-ratio and axon diameter in WT: 0.73 and 7.96 μm; Tbk1-LKO: 0.56 and 5.8 μm; Figure 1K-M).

mRNAs, including those of macrophage-related factors, were quantified, and we found that the mRNA levels of Mcp1, CD68 and Tnf-alpha showed a dramatic increase in the sciatic nerve of Tbk1-LKO mice compared with those in WT mice (Figure s3A). Therefore, we speculated that Tnf-alpha could induce motor neuron damage. However, neither human nor mouse Tnf-alpha damaged motor neuron-like cell lines, as evaluated by cell activity (human Tnf-alpha: 0.83±0.02 vs control: 0.8±0.02; mouse Tnf-alpha: 0.64±0.01 vs control: 0.72±0.05; Figure s3B-C). Interestingly, mouse Tnf-alpha combined with amlexanox (AML), which is a specific inhibitor of TBK1, significantly inhibited the activity of cells (mouse TNF+10

μM AML: 0.48±0.03; mouse TNF+100 μM AML: 0.28±0.01 vs control: 0.72±0.05), and cell activity was especially inhibited by addition of BV6 (0.19±0.0025 vs control: 0.72±0.05), which activates p52. Nik-smi1, a noncanonical NF-κB inhibitor, restored cell activity by 11.1% compared with that Tnf-alpha and AML were administered (0.3±0.02). These data supported that Tbk1 inefficiency combined with Tnf-alpha coinduced neuron degeneration that was partially rescued by a noncanonical NF-κB inhibitor. Furthermore, AML activated human leukemic monocytes (THP-1) at doses of 1 μM and 10 μM. NF-κB2 p52, which is a product of p100 processing, translocated into the nucleolus with RELB and induced the activation of noncanonical NF-κB pathways. Inhibition of Tbk1 activity by AML induced a two-fold increase in p52 generation in THP-1 cells (Figure s3D-F).

Tbk1-LKO induced intestinal tract inflammatory monocyte infiltration

Interestingly, we found that the intestinal tract was severely swollen in the Tbk1-LKO mice, especially in the small intestine (Figure 2A). Hematoxylin and eosin (HE) staining showed a large amount of inflammatory cells infiltrated in the mucous and submucous layers (Figure 2B). Flow cytometry analysis showed that the abundance of CD11b-positive cells with high expression of Ly6c significantly increased in the small intestine, both of which are markers of inflammatory monocytes (Figure 2C). Given that axonal pathology is related to inflammatory cell infiltration, CD11b expression was evaluated in the cortex, spinal cord, muscle, spleen, liver and small intestine. The level of CD11b was significantly increased in the small intestine in Tbk1-LKO mice (Figure 2D-E). The CD11b-positive cells aggregated on mainly the mucosa of the small intestine (Figure 2F). Macrophages in the small intestine are derived from monocytes and differentiate into M1 macrophages that highly express CD68 and Tnf-alpha and into M2 macrophages marked by Arg1 and Ym1 expression. Real-time PCR revealed that the levels of Arg1 and Ym1 were significantly reduced and that the levels of Tnf-alpha and CD68 did not show an increased tendency in the small intestine and colon in the Tbk1-LKO mice compared with those in WT mice (Figure 2G). We further performed immunostaining and immunoblotting to evaluate Arg1 expression in the small intestine. Arg1-positive cells were located mainly in the lamina propria of the small intestine. Consistent with the reduced level of Arg1 mRNA, Arg1 protein expression was also dramatically reduced in Tbk1-LKO mice (Figure s4A-C). Therefore, Tbk1 deletion in myeloid cells could induce inflammatory monocyte infiltration in the small intestine.

Next, enteric bacterial 16S sequencing was performed to determine whether Tbk1-LKO damaged the homeostasis of the microbiome in the gut. Indeed, the ratio of Firmicutes vs Bacteroidetes was reduced by 32% in the Tbk1-LKO mice compared with that in WT mice (Figure 2H-I, p=0.05). Through KEGG prediction, dysbacteroisis could be related to immune disease and neurodegenerative disease (Figure 2J).

The level of p-Tbk1 was reduced in inflammatory monocytes and microglia in ALS patients and animal models

Since Tbk1 deletion in myeloid cells led to nerve injury, the level of Tbk1 phosphorylation in leukocytes was tested by flow cytometry in ALS patients and an ALS animal model that overexpresses human mutant SOD1. Based on side and forward scatter patterns, we could determine three groups of cells,

lymphocytes (purple), granulocytes (blue) and monocytes (green). In particular, the monocytes had a higher level of p-Tbk1 than the granulocytes and lymphocytes (Figure 3A). Furthermore, the classical monocytes were gated by CD14 positive and CD16 negative signals, and we found that the mean fluorescent intensity (MFI) of p-Tbk1 was reduced by 29.5% and 14.8% in monocytes of definite ALS and probable ALS patients compared with that in monocytes of healthy subjects (Figure 3B, Figure s5A). In addition, 50% of ALS patients presented a lower level of p-TBK1 MFI than that in healthy subjects (Figure s5B). The level of p-Tbk1 was also analyzed by flow cytometry in the monocytes and microglia of ALS animals based on ly6c and cd11b expression, and p-Tbk1 was decreased by 27.6% and 45.5%, respectively (Figure 3C-E). Subsequently, spinal cord sections were stained for CD11b and p-Tbk1 at different stages (60 days, 90 days, and endstage), which showed that p-Tbk1 was located in mainly amoeboid microglia characterized by a round cell body and thin filopodium-like processes, with little p-Tbk1 in ramified inactive microglia. With the progression of disease, the abundance of activated microglia significantly increased in the spinal cord and did not overlap with p-Tbk1 signal (Figure 3F). Thus, the reduced level of p-Tbk1 in the monocyte-macrophage system could contribute to the pathogenesis of ALS.

Recent studies demonstrated that human endogenous retrovirus (HER-V) activation might be one of the causes of ALS. Therefore, the mRNA of HERV-Kevn, HERV-Kpol and HERV-Kgag and the mRNA of IFN-beta, TNF-alpha and MAVS, which are related to activation of the TBK1-IRF3-IFN-beta pathway, were evaluated by real-time PCR. Figure s6A shows that the level of IFN-beta mRNA decreased significantly with the increase in TNF-alpha in the monocytes of ALS patients. However, we did not find that HERV-K was activated in the monocytes (Figure s6B). The rate of inflammatory monocytes was also significantly increased in the ALS patients (Figure s6C). The monocytes of ALS patients were further differentiated into macrophages by using M-CSF, which showed a shedding cell process and increasing phagocytosis rate (Figure s6D-E).

PEI-mannose TBK1 extends survival of ALS transgenic mice

Considering that the level of p-Tbk1 was decreased in monocytes and microglia, the noncanonical NF-κB pathways could be activated in the ALS animal model. As shown in Figure 4A and Figure s7A, p52 was markedly increased in the ALS animal model, especially in microglia (Figure s7B). Therefore, we hypothesized that activated microglia, monocytes or macrophages expressing mutant SOD1 might be a potential therapeutic target. Moreover, we evaluated the distribution of PEI-mannose linked the p-EGFP-N1 plasmid targeting macrophages by intravenous injection. The rate of GFP-positive cells was 1.7%, 14.3% 15.8%, 26.3% and 18% among the CD206-positive cells in the blood, spinal cord, liver, spleen and small intestine, respectively (Figure 4B). The SaCas9-sgRNA5 system, which was used in our previous study and effectively deleted mutant SOD1 in motor neurons, was delivered by PEI-mannose at the presymptom stage of SOD1G93A mice. Surprisingly, the onset of disease was significantly delayed for 26 days, and the footprint and rotarod performance was markedly ameliorated (Figure 4D-G, video 1). However, the treatment did not significantly prolong the life span of SOD1G93A mice compared with that of the control mice (Figure 4H-I). Furthermore, PEI-mannose-TBK1 significantly prolonged survival, delayed weight loss

and preserved additional motor neurons in the SOD1 mutant mice (Figure 4J-K and Figure s8A-B, video 2).

Discussion

FTD is a heterogeneous neurodegenerative disease that often coexists with ALS. Several genetic alterations, including mutations in the Tbk1 gene, are common to both disorders. Tbk1 loss-of-function mutations have been shown to cause FTD and familial ALS[5], with reported frequencies of 1.1%, 3.4%, and 4.5% for these mutations in FTD, ALS, and FTD-ALS, respectively[19]. In this paper, we first reported that p-Tbk1 was reduced in monocytes and macrophages in sporadic ALS patients and in an SOD1 G93A animal model and that conditional deletion of Tbk1 in myeloid cells induced axonal nerve damage. Recent studies of Tbk1 conditional KO in B cells, T cells and dendritic cells have shown that Tbk1 regulates the homeostasis of immunity[13–15]. David R Beers and Stanley H Appel deeply reviewed the immune dysregulation in ALS and suggested that targeting the immune system could provide therapeutic strategies to ameliorate the pathogenesis of ALS[20]. ALS-related mutations (SOD1, TDP-43, C9, TBK1, OPTN, etc.) activated inflammatory responses and released inflammatory factors, including Tnf-alpha, Il-6, etc., eventually inducing motor neuron death[20–21]. Myeloid Tbk1 deletion induced inflammatory monocyte infiltration in the digestive tract and motor injury. PEI-mannose-TBK1 or PEI-mannose-AAV-SaCas9-sgRNA deleting mutant SOD1 in macrophages significantly delayed the disease onset and prolonged the survival of the SOD1 mutant animals. Thus, the inflammatory response caused by myeloid Tbk1 deficiency could contribute to the pathogenesis of ALS or FTD.

Several studies have supported that the gut microbiome could contribute to the pathogenesis of ALS and other neurodegenerative diseases. Eran Blacher et al demonstrated that Akkermansia muciniphila (AM) ameliorates whereas Ruminococcus torques and Parabacteroides distasonis exacerbates the symptoms of ALS[22]. The ALS mouse model presented a damaged tight junction structure and increased permeability[23]. In this paper, we found that Tbk1 deficiency in myeloid cells resulted in an intestinal microbiome shift, inflammatory monocyte infiltration and noncanonical NF-κB activation. The noncanonical NF-κB pathway selectively activates p100-sequestered NF-κB members, predominantly NF-κB2 p52 and RELB[24]. Shao-Cong Sun has deeply reviewed the role of noncanonical NF-κB in inflammation and immunity and elucidated that the noncanonical NF-κB pathway is slow and persistently activated by the ligands of a subset of tumor necrosis factor receptor (TNFR) superfamily members[25–26]. The slow progression with chronic inflammatory cell infiltration is the most prominent feature of ALS or FTD. Thus, enhancing TBK1 activity in macrophages could be a potential therapeutic target to control inflammatory cell infiltration and regulate the intestinal microorganism balance for ALS or FTD.

Conclusions

Our results suggest that inflammatory monocyte and macrophage infiltration and impaired innate immune defense are contributing factors to ALS and FTD and enhancing TBK1 activity could be a potential therapeutic target for patients related with ALS or FTD.

Abbreviations

ALS:amyotrophic lateral sclerosis; FTD:frontotemporal dementia; Tbk1:TANK-binding kinase1; IKK:IκB kinase; Tbk1-LKO:Tbk1fl/fl LysMcre ; WT:wild-type; AML:amlexanox; THP-1:human leukemic monocytes; MFI:mean fluorescent intensity; HER-V:human endogenous retrovirus; AM:Akkermansia muciniphila; TNFR:tumor necrosis factor receptor.

Declarations

Acknowledgements

We thank the Electron Microscopy, Confocal Microscopy and Cytomics Services at the Neurological Laboratory of Hebei Province.

Funding

This work was supported by grants from the Natural Science Foundation of China (31371089, 81171210).

Availability of data and materials

Not applicable

Authors' contributions

Weisong Duan, and Chunyan Li conceived and designed the experiments. Le Yi, Yunyun Tian, Zhongyao Li, Yue Bi, Yuanyuan Li and Yakun Liu performed the biochemical experiments and analyzed the data. Huai-peng Huang and Yanqin Ma performed the RT-PCR studies animal experiments. Weisong Duan, Xueqin Song, Yaling Liu and Chunyan Li wrote and revised the manuscript. All authors read and approved the final manuscript.

Ethics approval and consent to participate

Animal experiments were carried out according to the laboratory animal management regulations promulgated by the Ministry of Science and Technology of the People's Republic of China, which are in accordance with the NIH Guide for the Care and Use of Laboratory Animals.

Consent for publication

Not applicable.

Competing interests

The authors declare that they have no competing interests.

References

1. Taylor JP, Brown RH Jr, Cleveland DW. Decoding ALS: from genes to mechanism. Nature 2016; 539:197-206.
2. Navone F, Genevini P, Borgese N. Autophagy and Neurodegeneration: Insights from a Cultured Cell Model of ALS. Cells. 2015;4(3):354-86.
3. Cirulli ET, Lasseigne BN, Petrovski S, et al. Exome sequencing in amyotrophic lateral sclerosis identifies risk genes and pathways. Science. 2015;347(6229):1436-41.
4. Freischmidt A, Wieland T, Richter B, et al. Haploinsufficiency of TBK1 causes familial ALS and fronto-temporal dementia. Nat Neurosci. 2015;18(5):631-6.
5. Freischmidt A, Müller K, Ludolph AC, Weishaupt JH, Andersen PM. Association of Mutations in TBK1 With Sporadic and Familial Amyotrophic Lateral Sclerosis and Frontotemporal Dementia. JAMA Neurol. 2017;74(1):110-113.
6. Lomen-Hoerth C, Anderson T, Miller B. The overlap of amyotrophic lateral sclerosis and frontotemporal dementia.Neurology. 2002;59(7):1077-9.
7. van der Zee J, Gijselinck I, Van Mossevelde S, Perrone F, Dillen L, Heeman B, Bäumer V, Engelborghs S, De Bleecker J, Baets J, Gelpi E, Rojas-García R, Clarimón J, Lleó A, Diehl-Schmid J, Alexopoulos P, Perneczky R, Synofzik M, Just J, Schöls L, Graff C, Thonberg H, Borroni B, Padovani A, Jordanova A, Sarafov S, Tournev I, de Mendonça A, Miltenberger-Miltényi G, Simões do Couto F, Ramirez A, Jessen F, Heneka MT, Gómez-Tortosa E, Danek A, Cras P, Vandenberghe R, De Jonghe P, De Deyn PP, Sleegers K, Cruts M, Van Broeckhoven C, Goeman J, Nuytten D, Smets K, Robberecht W, Damme PV, Bleecker J, Santens P, Dermaut B, Versijpt J, Michotte A, Ivanoiu A, Deryck O, Bergmans B, Delbeck J, Bruyland M, Willems C, Salmon E, Pastor P, Ortega-Cubero S, Benussi L, Ghidoni R, Binetti G, Hernández I, Boada M, Ruiz A, Sorbi S, Nacmias B, Bagnoli S, Sorbi S, Sanchez-Valle R, Llado A, Santana I, Rosário Almeida M, Frisoni GB, Maetzler W, Matej R, Fraidakis MJ, Kovacs GG, Fabrizi GM, Testi S. TBK1 Mutation Spectrum in an Extended European Patient Cohort with Frontotemporal Dementia and Amyotrophic Lateral Sclerosis. Hum Mutat. 2017;38(3):297-309.
8. Marchlik, P. Thakker, T. Carlson et al., “Mice lacking Tbk1 activity exhibit immune cell infiltrates in multiple tissues and increased susceptibility to LPS-induced lethality,” Journal of Leukocyte Biology, vol. 88, no. 6, pp. 1171–1180, 2010.
9. Sharma S, tenOever BR, Grandvaux N, Zhou GP, Lin R, Hiscott J. Triggering the interferon antiviral response through an IKK-related pathway. Science. 2003 May 16;300(5622):1148-51. Epub 2003 Apr 17.
10. Zhao P, Wong KI, Sun X, Reilly SM, Uhm M, Liao Z, Skorobogatko Y, Saltiel AR. TBK1 at the Crossroads of Inflammation and Energy Homeostasis in Adipose Tissue. Cell. 2018 Feb

8;172(4):731-743.e12.

11. Muñoz MC, Giani JF, Mayer MA, Toblli JE, Turyn D, Dominici FP. TANK-binding kinase 1 mediates phosphorylation of insulin receptor at serine residue 994: a potential link between inflammation and insulin resistance. J Endocrinol. 2009 May;201(2):185-97. doi: 10.1677/JOE-08-0276. Epub 2009 Feb 27.
12. Bonnard M, Mirtsos C, Suzuki S, Graham K, Huang J, Ng M, Itié A, Wakeham A, Shahinian A, Henzel WJ, Elia AJ, Shillinglaw W, Mak TW, Cao Z, Yeh WC. Deficiency of T2K leads to apoptotic liver degeneration and impaired NF-kappaB-dependent gene transcription. EMBO J. 2000;19(18):4976-85.
13. Jin J, Xiao Y, Chang JH, Yu J, Hu H, Starr R, Brittain GC, Chang M, Cheng X, Sun SC.The kinase TBK1 controls IgA class switching by negatively regulating noncanonical NF-κB signaling. Nat Immunol. 2012;13(11):1101-9.
14. Yu J, Zhou X, Chang M, Nakaya M, Chang JH, Xiao Y, Lindsey JW, Dorta-Estremera S, Cao W, Zal A, Zal T, Sun SC.Regulation of T-cell activation and migration by the kinase TBK1 during neuroinflammation. Nat Commun. 2015;6:6074.
15. Xiao Y, Zou Q, Xie X, Liu T, Li HS, Jie Z, Jin J, Hu H, Manyam G, Zhang L, Cheng X, Wang H, Marie I, Levy DE, Watowich SS, Sun SC.The kinase TBK1 functions in dendritic cells to regulate T cell homeostasis, autoimmunity, and antitumor immunity.J Exp Med. 2017;214(5):1493-1507.
16. Duan W, Guo M, Yi L, Zhang J, Bi Y, Liu Y, Li Y, Li Z, Ma Y, Zhang G, Liu Y, Song X, Li C. Deletion of Tbk1 disrupts autophagy and reproduces behavioral and locomotor symptoms of FTD-ALS in mice. Aging (Albany NY). 2019 Apr 30;11(8):2457-2476.
17. Steele AJ, Al-Chalabi A, Ferrante K, Cudkowicz ME, Brown RH Jr, Garson JA. Detection of serum reverse transcriptase activity in patients with ALS and unaffected blood relatives. Neurology. 2005 Feb 8;64(3):454-8.
18. Li W, Lee MH, Henderson L, Tyagi R, Bachani M, Steiner J, Campanac E, Hoffman DA, von Geldern G, Johnson K, Maric D, Morris HD, Lentz M, Pak K, Mammen A, Ostrow L, Rothstein J, Nath A. Human endogenous retrovirus-K contributes to motor neuron disease. Sci Transl Med. 2015 Sep 30;7(307):307ra153.
19. Gijselinck I, Van Mossevelde S, van der Zee J, Sieben A, Philtjens S, Heeman B, Engelborghs S, Vandenbulcke M, De Baets G, Bäumer V, Cuijt I, Van den Broeck M, Peeters K, Mattheijssens M, Rousseau F, Vandenberghe R, De Jonghe P, Cras P, De Deyn PP, Martin JJ, Cruts M, Van Broeckhoven C; BELNEU Consortium.Loss of TBK1 is a frequent cause of frontotemporal dementia in a Belgian cohort.Neurology. 2015;85(24):2116-25.
20. Beers DR, Appel SH. Immune dysregulation in amyotrophic lateral sclerosis: mechanisms and emerging therapies. Lancet Neurol. 2019 Feb;18(2):211-220.
21. Frakes AE, Ferraiuolo L, Haidet-Phillips AM, Schmelzer L, Braun L, Miranda CJ, Ladner KJ, Bevan AK, Foust KD, Godbout JP, Popovich PG, Guttridge DC, Kaspar BK. Microglia induce motor neuron death via the classical NF-κB pathway in amyotrophic lateral sclerosis. Neuron. 2014;81(5):1009-1023.

22. Blacher E, Bashiardes S, Shapiro H, Rothschild D, Mor U, Dori-Bachash M, Kleimeyer C, Moresi C, Harnik Y, Zur M, Zabari M, Brik RB, Kviatcovsky D, Zmora N, Cohen Y, Bar N, Levi I, Amar N, Mehlman T, Brandis A, Biton I, Kuperman Y, Tsoory M, Alfahel L, Harmelin A, Schwartz M, Israelson A, Arike L, Johansson MEV, Hansson GC, Gotkine M, Segal E, Elinav E. Potential roles of gut microbiome and metabolites in modulating ALS in mice. Nature. 2019 Aug;572(7770):474-480.
23. Wu S, Yi J, Zhang YG, Zhou J, Sun J. Leaky intestine and impaired microbiome in an amyotrophic lateral sclerosis mouse model. Physiol Rep. 2015 Apr;3(4). pii: e12356.
24. Xiao, G., Harhaj, E. W. & Sun, S. C. NF-κB-inducing kinase regulates the processing of NF-κB2 p100. Mol. Cell 7, 401–409 (2001).
25. Sun SC. The non-canonical NF-κB pathway in immunity and inflammation. Nat Rev Immunol. 2017 Sep;17(9):545-558.
26. Shi JH, Xie X, Sun SC. TBK1 as a regulator of autoimmunity and antitumor immunity. Cell Mol Immunol. 2018 Aug;15(8):743-745.

Supplementary Files Legend

Fig s1 (A) Common data about Tbk1-LKO mice. (B) The gastrocnemius fiber area of Tbk1-LKO mice and WT mice, n=253-281.

Fig s2 Neu N, Chat, GFAP and IBA1 staining in the spinal cord of Tbk1-LKO and WT mice.

Fig s3 A Tbk1 activity inhibitor induced NSC-34 damage and p52 activation in THP-1 cells. (A) Mcp-1, Tnf-alpha, CD68, Ym-1 and Arg-1 mRNA levels were quantified in the sciatic nerve (SN) of Tbk1-LKO and WT mice (n=3, *P < 0.05, Tbk1-LKO vs WT). (B-C) Measurement of NSC-34 cell viability after treatment with AML (0, 10, 100 mM), human TNF-alpha (200, 500 ng/mL), mouse Tnf-alpha (100, 500 ng/mL), BV6 (10mM) and Nik smi1 (10 mM) (n=3, *P < 0.05, Tbk1-LKO vs WT). (D) Measurement of THP-1 cell viability after treatment with AML (0, 10, 100 mM) (n=3, *P < 0.05, Tbk1-LKO vs WT). (E-F) The expression of p52 was evaluated by Western blot (n=3, *P < 0.05, Tbk1-LKO compared to WT).

Fig s4 (A, C) Arginase-1 (Arg 1) expression in the cortex (co), spinal cord (sp), muscle (mu), spleen (spl), liver (li) and small intestine (si). n=3, *P < 0.05, compared to WT control. (B) Arginase-1 staining in the small intestine, n=3, bar=50 mm.

Fig s5 (A-B) MFI and frequency of p-TBK1 in the monocytes of healthy, definite ALS and probable ALS subjects.

Fig s6 (A) IFN-beta, TNF-alpha, MAVS, HERV-Kenv, HERV-Kpol, and HERV-Kgag mRNA levels were evaluated in the monocytes of ALS patients. (B) The rate of CD14-positive and CD16-negative inflammatory monocytes in the ALS patients and controls. (C-D) Representative images of macrophages.

Fig s7 P100/52 statisticallya analysis, n=3, *P < 0.05 (A) P100/52 distribution in the spinal cord (B), n=3, bar=50 mm.

Fig s8 (A-B) NeuN and IBA1 staining and analysis of motor neurons in the spinal cord of SOD1G93A mice treated with PEI-mannose-TBK1, n=3, bar=50 mm, *P < 0.05, compared to WT control.

Table s1 Common data for ALS and healthy subjects.

Table s2 Primers used in this paper.

Video 1 The locomotor activity of mice treated with PEI-mannose-AAV-SaCas9-sgRNA targeting SOD1 was recorded at 120 days of age.

Video 2 The locomotor activity of mice treated with PEI-mannose-TBK1 was recorded at 120 days of age.

Figures

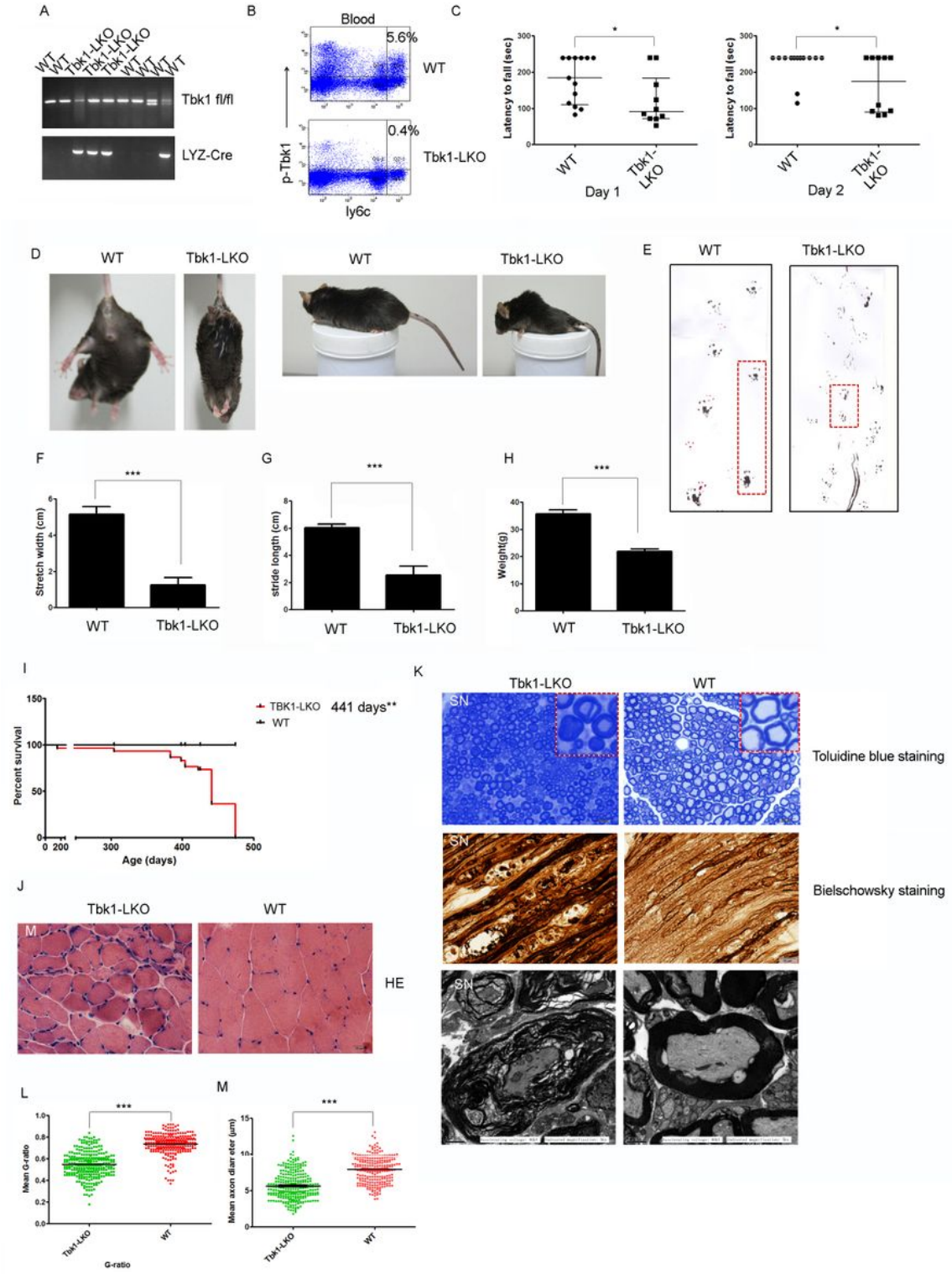

Figure 1

Behavioral and pathological evaluation of Tbk1-LKO mice. (A) Tbk1-LKO mice were established by crossing Tbk1fl/fl mice with LysM-cre mice and genotyped by PCR. (B) p-Tbk1 was analyzed by cytometry flow in ly6c-positive cells. (C) The locomotor activity of 7-month-old Tbk1-LKO mice (n = 10-13, *P < 0.05, compared to WT control). (D-E) Clasping and footprint assessment. (F-G) Stretch width and stride length measurements (n =5, ***P < 0.001, Tbk1-LKO vs WT). (H) Body weight (n=5, ***P < 0.001,

Tbk1-LKO vs WT). (I) Survival rate of Tbk1-LKO mice (n=19-39, **P < 0.01, Tbk1-LKO vs WT). (J) HE staining of gastrocnemius fiber (n=3). (K) Toluidine blue staining (bar = 20 μm), Bielschowsky staining (bar = 10 μm) and electronic microscopy images (bar = 2 μm) of the sciatic nerve (n=5). (L-M) Mean G-ratio and axonal diameter analysis in Tbk1-LKO and WT mice (SN: sciatic nerve; n=5; ***P < 0.001, compared to WT control).

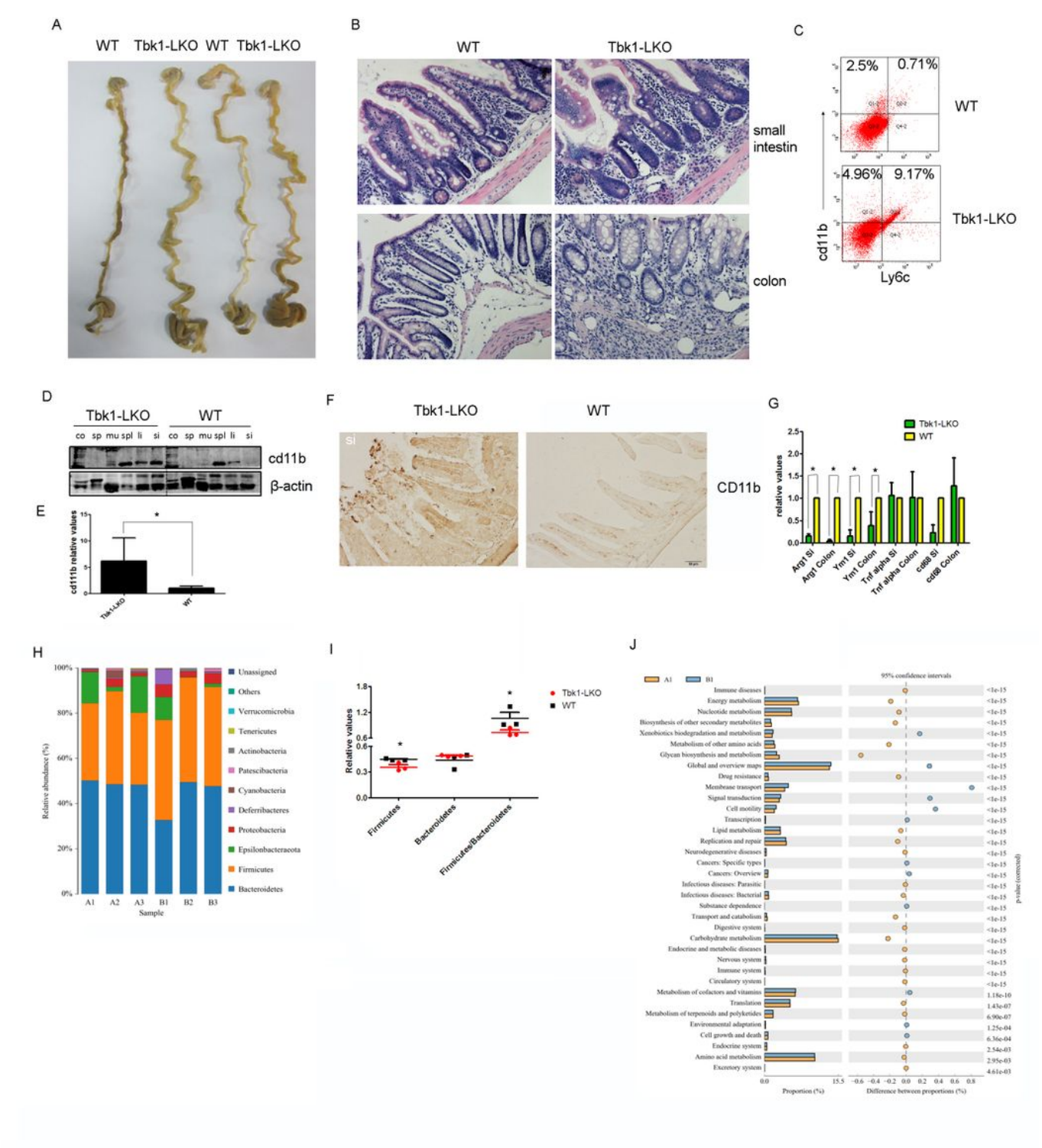

Figure 2

Inflammatory cell infiltration in the digestive tract of Tbk1-LKO mice. (A-B) The digestive tract appearance and HE staining (n=3). (C) The inflammatory monocytes marked by ly6c and CD11b double positive signals were analyzed by cytometry flow, n=3. (D-F) cd11b expression and distribution in the cortex (co), spinal cord (sp), muscle (mu), spleen (spl), liver (li) and small intestine (si). n=3, *P < 0.05, compared to WT control. (G) The mRNA of Tnf-alpha, CD68, Ym-1 and Arg-1 was quantified in the small intestine (si) and colon of Tbk1-LKO and WT mice (n=3, *P < 0.05, Tbk1-LKO vs WT). (H-J) The 16S DNA was sequenced in the fecal extracts of age-matched WT and Tbk1-LKO mice(n = 3, *P < 0.05, compared to WT control).

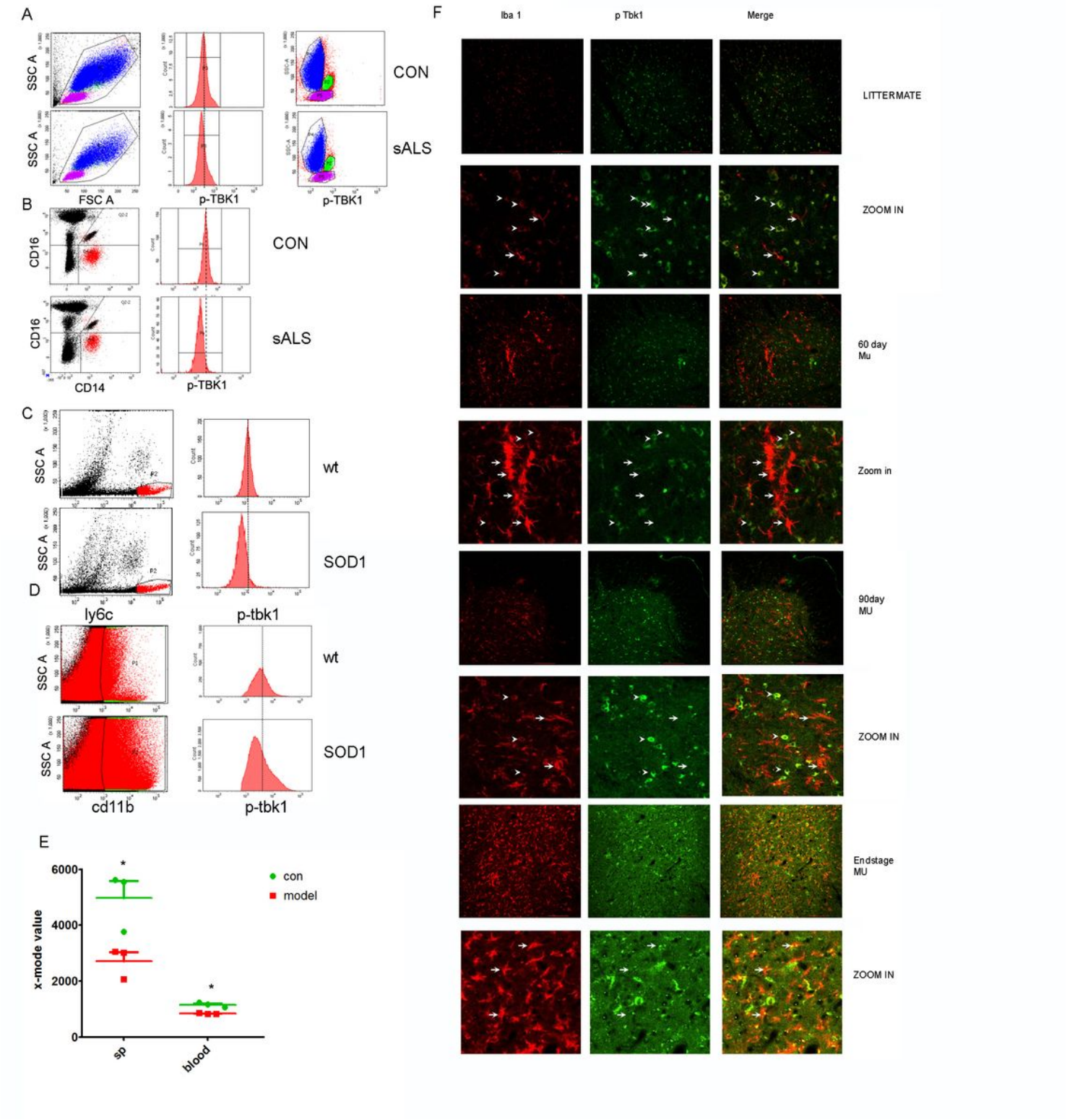

Figure 3

The level of p-Tbk1 was evaluated in the monocytes and macrophages of ALS patients and an animal model. (A-B) p-Tbk1 content was analyzed in CD16-negative and CD14-positive classic monocytes from ALS patients and age-matched healthy subjects (n=12-15). (C-E) The evaluation of p-Tbk-1 content in monocytes and macrophages of an ALS animal model, n=3, *P < 0.05, compared to WT control. (F) The distribution of p-Tbk1-positive microglia in the spinal cord of the ALS animal model (n=3). Bar = 100 □m.

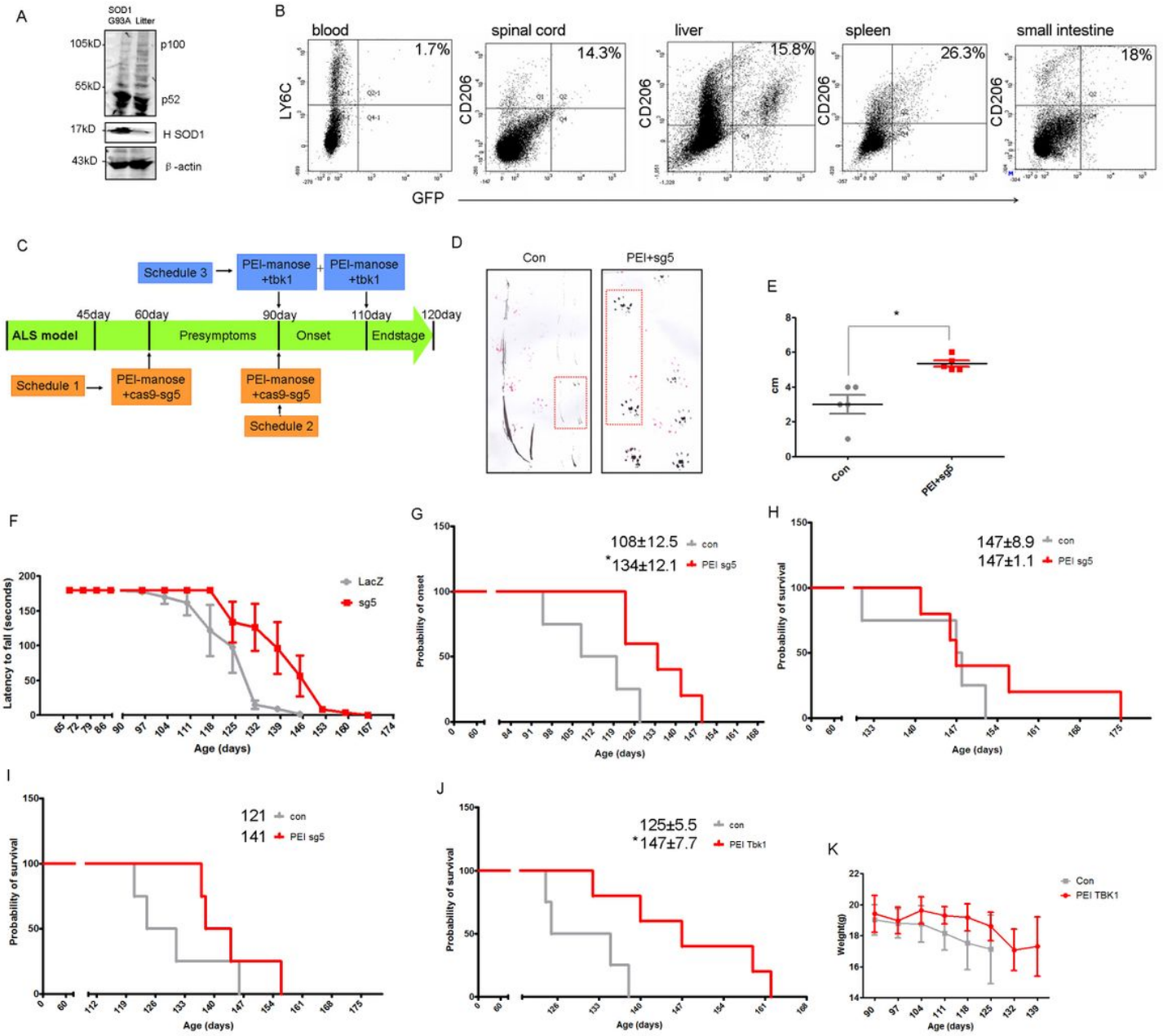

Figure 4

Targeting macrophages for treatment in the ALS model. (A) p52 expression in the ALS model (n=3). (B) Evaluation of GFP expression in macrophages by a PEI-mannose-packaged p-EGFP vector, with CD206 positivity marking macrophages. (C) Schedules of treatment for the ALS animal model. (D, E) Footprints of transgenic mice treated with PEI-mannose-AAV-SaCas9-sgRNA targeting SOD1 or with a 0.9% normal saline control, as measured at 120 days of age. (F) The latency to fall in the mice treated with PEI-mannose-AAV-SaCas9-sgRNA and in the control mice was evaluated. *P<0.05 compared with the control group. (G-H) Disease onset (G) and survival rate (H) of SOD1G93A mice treated with PEI-mannose-AAV-SaCas9-sgRNA at the age of 60 days (median±SE, n=5,*P<0.05 compared with the control group). (F-G):

Survival rate of SOD1G93A mice treated with PEI-mannose-AAV-SaCas9-sgRNA at the age of 90 days (median±SE, n=6). (J) Survival rate of SOD1G93A mice treated with PEI-mannose-TBK1 at the age of 90 days (median±SE, n=5, *P<0.05 compared with the control group). (K) The weights of the mice treated with PEI-mannose-TBK1 and the control mice (n=5) were evaluated.

Supplementary Files

This is a list of supplementary files associated with this preprint. Click to download.

- Figs2chatcopy.jpg
- video1MVI6509sg5m.mp4
- video2MVI6518tbk190day.mp4
- figs6copy.jpg
- Figs7.jpg
- figs1commandatatbk1lkocopy.jpg.jpg
- figs5distributionptbk1humancopy.jpg
- figs4ARG1copy.jpg
- figs3fig2copy.jpg
- tables2primer1.docx
- tables1alspateints1.docx
- figs8copy.jpg